Fish-Inspired Nanostructured Lubricated Surfaces Enhance Aquatic Locomotion

CHEMISTRY OF MATERIALS

pubs.acs.org/cm

Article

Fish-Inspired Nanostructured Lubricated Surfaces Enhance Aquatic Locomotion

Published as part of Chemistry of Materials special issue "Celebrating the Legacy of Edwin Chandross".

Jack Alvarenga, Mughees Khan, Patrick J. M. Thornycroft, Dylan K. Wainwright, Li Wen, Erik J. Anderson, Philseok Kim, George V. Lauder, and Joanna Aizenberg*

Cite This: https://doi.org/10.1021/acs.chemmater.6c01113

Read Online

ACCESS | Metrics & More | Article Recommendations | Supporting Information

ABSTRACT: Slippery, mucus-coated body surfaces are widespread in aquatic vertebrates, but their contribution to locomotion is unclear. Fish mucus has long been proposed to reduce drag, yet direct experimental evidence of a swimming benefit is limited. A series of four mucus-inspired, lubricant-infused aluminum substrates incorporating SLIPS (slippery liquid-infused porous surfaces) were fabricated to assess the effects of a slippery coating on motion under both static (drag-based) and dynamic (propulsive) conditions. The aluminum substrates were textured by conversion of the surface to nanostructured aluminum oxyhydroxide (boehmite), chemically functionalized, and infused with synthetic Newtonian liquids spanning the viscosity range of measured trout mucus and compared to that of unstructured and lubricant-free controls. Viscosity measurements were also performed on skin mucus collected from brook trout (*S. fontinalis*). SLIPS-coated surfaces were found to reduce the static drag by up to 9.1% and enhance the lift-to-drag ratio by up to 8.7%. Furthermore, SLIPS coatings improved both the thrust and efficiency of flapping plates actuated in heave and pitch by up to 3.6% and 4.1%, respectively, with performance improvements observed over a broad range of motion parameters, lubricant chemistries, and viscosities. Boundary layer flow measurements over a flat plate revealed that SLIPS experienced a reduced skin friction drag of up to 5.2% under laminar flow conditions. Nanostructured, functionalized, lubricated coatings thus act both to reduce drag and to enhance the propulsive thrust and efficiency of fishlike propulsion, providing one explanation for the presence of such structures on a diversity of animal surfaces.

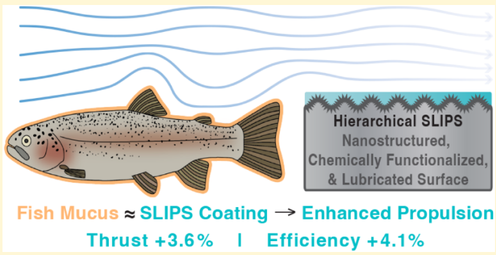

■ INTRODUCTION

Slippery surfaces are ubiquitous in nature, manifesting in biological films that develop on both natural and engineered material surfaces where fluids interact with a substrate,[1] mucus-lined biological passageways,[2] hydrophilic plant surfaces,[3] and the mucus-coated surfaces of many animals, such as fish, that inhabit the comparatively viscous aquatic medium.[4,5] Such surfaces represent a fundamental interfacial phenomenon, serving as the locus of fluid-substrate interactions that are critical to biological function. These interactions govern the transfer of cellular metabolites and gases as well as the generation of frictional forces on bodies moving through fluids.[6−8]

The mucus coating of fishes has attracted considerable attention as a slippery surface that functions as a key component of the immune system,[9] can play a role in predatory defense,[5] and may act to reduce hydrodynamic drag during locomotion.[7,10−13] Direct experimental measurement of drag on *Paramisgurnus dabryanus* loach skin has demonstrated 28% drag reduction attributable to the presence of mucus.[14] Biomimetic lubricant-infused surfaces inspired by the reentrant mucus storage anatomy of loach, hagfish, and seaweed have been shown to exceed 20% frictional drag reduction under certain conditions while maintaining lubricant stability under repeated exposure to high shear flow, a property attributed to lubricant recirculation within the reentrant cavity structure that mimics the continuous mucus renewal by goblet cells in fish skin.[15−17] The textured surface of fish scales has also been proposed to aid in retaining the mucus layer on the body surface against external fluid flows,[12,14,18−20] and the locomotor role of fish mucus has received particular interest as a potential mechanism for reducing drag and, consequently, the energetic cost of movement.[21]

Numerical simulations of undulatory foil propulsion with shear-thinning non-Newtonian interfaces and Navier slip boundary conditions modeled on fish mucus have demonstrated reductions in friction drag and enhancements in thrust and

Received: April 16, 2026
Revised: July 23, 2026
Accepted: July 27, 2026

propulsive efficiency.[11,22] When validated against boundary layer velocity measurements on a slippery, seaweed-covered surface, a reduction in power input by up to 8% and an improvement in propulsive efficiency by up to 7% during flapping propulsion were observed.[22] However, direct experimental demonstration of thrust and efficiency improvements under physically realistic propulsive conditions has not been studied. A mucus coating could alter the boundary layer flow profile by introducing an effective slip condition at the body surface, modifying the near-wall velocity gradient, and reducing skin friction drag. This effect may be further supplemented by the gradual shedding of mucus into the passing flow. Fish locomotion involves an oscillatory body;[23,24] therefore, a comprehensive evaluation of the locomotor benefits of a slippery surface must incorporate both static analyses of drag and lift forces as a function of the surface structure and chemistry to assess surface effects, alongside dynamic testing during oscillatory propulsion to mimic the heaving and pitching motions of fish swimming.[25]

To address this experimental gap, the slippery liquid-infused porous surface (SLIPS) coating platform,[26,27] also commonly referred to as liquid-infused surfaces (LIS), was employed as a well-characterized bioinspired model of a slippery interface. SLIPS incorporate a lubricant infused into a textured and chemically functionalized surface structure designed to minimize lubricant loss. Superhydrophobic surfaces were also fabricated for comparison to SLIPS coatings and uncoated control surfaces. The principle of trapping an immiscible liquid layer at an interface to repel other liquids has led to a broad range of SLIPS applications, including reduced adhesion and high repellency of ice,[28,29] blood,[30] and marine organisms,[31,32] as well as the prevention of bacterial biofilms[33] and the reduction of corrosion.[34,35] Studies of the viscosity ratio between infusing and external liquids report drag reductions of 16% in laminar rheometer flow[36] and 14% in turbulent Taylor-Couette flow,[37] rising to 35% on lubricant-infused surfaces when feature dimensions, fluid area fraction, and Reynolds number (*Re*) are also considered.[38] In numerical simulations, micropore lubricant-infused surfaces modeled after the mucus storage anatomy of fish and seaweed have demonstrated drag reductions of up to 22.6% at a high flow velocity, with performance governed by the cavity open area fraction, lid thickness, and the resulting lubricant dispersion patterns.[39]

The goal of this study is to quantify the locomotor effects of exemplary slippery surface coatings with different chemical and structural compositions during fish-like propulsion using an experimental platform that enables direct measurement of propulsive thrust and efficiency. Nanoscale and hierarchically textured SLIPS infused with synthetic Newtonian liquids spanning the viscosity range of fish mucus are employed to directly test whether a lubricious surface coating alters thrust and efficiency during propulsion. Both static and dynamic hydrodynamic tests were conducted across a broad range of motion parameters to assess whether and to what extent a mucus-like lubricated surface confers a measurable and robust performance advantage over an uncoated control, with static measurements of lift and drag forces providing a mechanistic basis for interpreting the dynamic swimming results.

■ RESULTS

Rigid aluminum alloy plates were fabricated with SLIPS coatings through hierarchical or nanoscale texturization, chemical functionalization, and infusion with one of two lubricants of differing viscosity (Figure 1), as described in the Materials and Methods. Nanostructuring occurs through the conversion of the

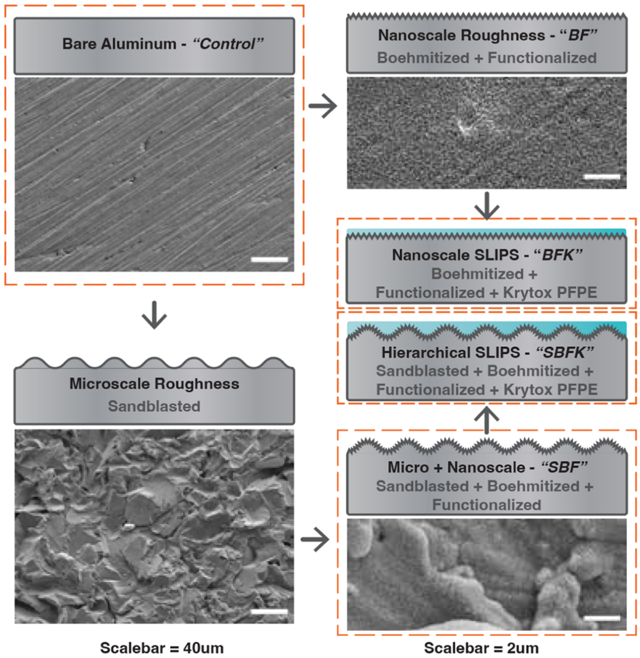

Figure 1. Fabrication pathways and scanning electron micrographs of the four tested aluminum plate surfaces. The four surfaces used in hydrodynamic testing (highlighted by orange dashed boxes) were produced through sequential surface preparation steps. The *Control* surface is bare 6061 aluminum alloy with an average surface roughness of 0.06 μm.[19] The *BFK* (nanoscale SLIPS) surface was produced by boehmitization of bare aluminum to form a uniform aluminum oxyhydroxide (AlO(OH)) nanoscale texture (~200 nm), followed by chemical functionalization and infusion with a perfluoropolyether (PFPE) lubricant (Krytox). The *SBF* (superhydrophobic) surface was produced by sandblasting bare aluminum to generate microscale roughness, followed by boehmitization to create hierarchical micro- and nanoscale texture, and chemical functionalization; this surface was not infused with lubricant. The *SBFK* (hierarchical SLIPS) surface was produced by infusing the SBF surface with PFPE lubricant. Schematic cross-sections above each SEM image illustrate the surface texture profile and lubricant layer (teal) where present. Scale bars: 40 μm for left images and 2 μm for right images.

surface layer of the aluminum plates to boehmite (aluminum oxyhydroxide, AlO(OH)) in a process called boehmitization.[40] Both static and propulsive tests were conducted on coated aluminum plates relative to a smooth, uncoated control plate, with an average surface roughness of 0.06 μm (Supplemental Movies S1, S2; Table S1).

Three modified surface types were tested relative to the control, designated here as SBF, BFK, and SBFK. SBF (Sandblasted + Boehmitized + Functionalized) plates were textured at two length scales (first by sandblasting at a micron scale and then boehmitized to create a top nanoscale layer), chemically functionalized with a fluoroaliphatic phosphoric acid, but not infused with a lubricant, forming a superhydrophobic surface control. During chemical functionalization, the phosphoric acid headgroup forms a strong bond with AlO(OH) through ligand exchange at hydroxyl sites on the boehmite surface, positioning the perfluoroalkyl tails at the interface with water.[41−47] The boehmite nanoscale layer is particularly well-suited for this functionalization chemistry: its crystal structure

https://doi.org/10.1021/acs.chemmater.6c01113
Chem. Mater. XXXX, XXX, XXX−XXX

exposes a high surface density of Al−OH hydroxyl groups, which serve as anchoring sites for phosphate esters.[48,49] The density and spatial geometry of these surface hydroxyl groups directly determine the surface coverage of the fluorinated functionalization layer and consequently the capacity of the surface to maintain a continuous lubricant layer under flow.[50,51] In this case, the fluorinated alkyl chains render the surface oleophilic/fluorophilic, creating thermodynamic affinity for the perfluoropolyether (PFPE) lubricant (Krytox).[26] This surface−lubricant affinity is what distinguishes SLIPS from a simple liquid film, providing the energetic driving force for lubricant retention against shear-driven drainage. BFK (Boehmitized + Functionalized + Krytox) plates were textured at the nanoscale, functionalized, and infused with either Krytox 100 or Krytox 103 lubricant (the latter approximately six times more viscous) to form a SLIPS-coated surface. SBFK (Sandblasted + Boehmitized + Functionalized + Krytox) plates were textured at two length scales and functionalized (similar to SBF samples) and further infused with either Krytox 100 or Krytox 103 to form a second set of SLIPS-coated surfaces (Figure 1; Tables S1, S2). PFPE lubricants are chemically inert, immiscible with water, and nonvolatile, making them stable candidates for studies of aqueous interfacial phenomena.[52,53]

Viscosity (μ) measurements of the Krytox lubricants and trout mucus relative to deionized water are presented in Figure 2. The average viscosities of Krytox 100 and Krytox 103 lubricants were 20 mPa·s and 120 mPa·s, respectively. The viscous properties of trout mucus depend on the extent to which water is removed by centrifugal dewatering prior to testing. Mucus sampled directly from live fish contains additional water from the fish surface and displays Newtonian behavior over 2 orders of magnitude of shear rate, with an average viscosity of 4 mPa·s. Centrifugation to remove low-viscosity components yields trout mucus exhibiting marked shear-rate dependence (Figure 2), with an average viscosity of 18 mPa·s over the tested shear rate range. The two Krytox SLIPS lubricants thus bracket the viscosity exhibited by dewatered trout mucus at shear rates up to 40 s^{-1}. With the biological and rheological context established, the hydrodynamic performance of these surfaces was evaluated under both static and dynamic conditions.

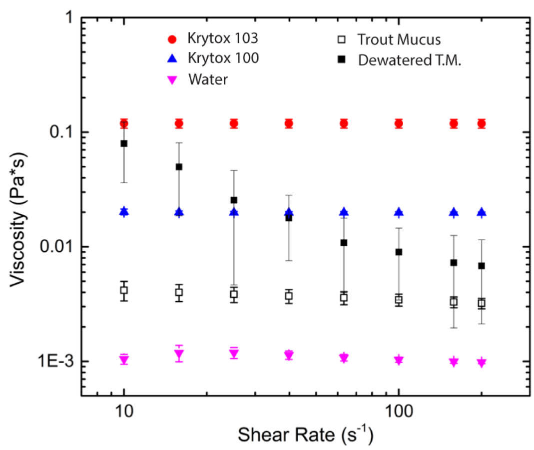

Figure 2. Viscosity of synthetic lubricants and brook trout (*Salvelinus fontinalis*) mucus as a function of shear rate, measured by rheometry (log−log scale). Krytox 103 (120 mPa·s) and Krytox 100 (20 mPa·s) exhibit Newtonian behavior across the full range of shear rates tested. As-collected trout mucus (open squares) also exhibits approximately Newtonian behavior, with a mean viscosity of 4 mPa·s. Centrifuged dewatered trout mucus (filled squares) displays marked shear-thinning behavior, with a mean viscosity of 18 mPa·s at low shear rates, bracketed by the two Krytox lubricants. Deionized water is shown for reference (inverted triangles). Error bars represent standard deviation from at least three independent measurements.

At a 0° angle of attack, SLIPS-coated plates (BFK and SBFK) exhibit greater drag reduction than the superhydrophobic surface (SBF) at Reynolds numbers (Re) between 20,000 and 40,000 (Figure 3). Over this Reynolds number range, BFK 100 and SBFK 100 plates achieved average drag reductions of 9.1 (±3.5) % and 8.4 (±3.2) %, respectively, compared to 4.4 (±3.5) % for the SBF surface (Table 1). Propagated standard errors on these derived drag reduction values are substantial (Figure 3, bottom panels), and with one exception, no individual data point is statistically distinguishable from zero at the $p < 0.05$ level. The sole statistically significant result is SBFK 100 at Re = 25,000, which is consistent with the peak drag reduction observed near this Reynolds number across all surface types. The evidence for drag reduction across the broader Re range therefore rests primarily on the consistent positive trend across all tested Re values and surface types, rather than on the statistical significance of individual points.

SLIPS-coated surfaces also enhance the lift-to-drag (L/D) ratio of the rigid plates at higher angles of attack (Figure 4; Supplemental Movie S1). Lift and drag forces were measured at a flow speed of 0.25 m/s up to an angle of attack of 20°, beyond which substantial flow separation over the plate surface was observed. The lift-to-drag ratio was evaluated for BFK and SBFK plates infused with lubricants of two different dynamic viscosities, Krytox 100 (20 mPa·s at 25 °C) and Krytox 103 (120 mPa·s at 25 °C). All SLIPS yielded an increase in the lift-to-drag ratio across the full range of angles examined (Figure 4). A peak L/D ratio of approximately 4 occurs at a 7° angle of attack, at which all SLIPS plates exhibit an increase in the peak lift-to-drag ratio of between 4.3 (±0.8)% and 8.7 (±0.8)% relative to the uncoated control (Table 1), with the greatest performance improvement of 8.7% achieved by the hierarchically textured SBFK 100 plate. The L/D improvement is most statistically robust near the peak L/D angle of 7°, where separation between the coated and control polynomial fits is greatest and propagated errors on the derived L/D improvement are smallest relative to the effect size (Figure 4, bottom row insets). At very low angles of attack (below ∼5°), the percentage L/D improvement shown in the bottom insets should be interpreted with caution for two compounding reasons. First, near 0°, the L/D ratio of the control surface approaches zero, making the denominator of the percentage calculation near-singular and the resulting values mathematically unstable. Second, in the range of approximately 2−5°, where the drag reduction values in the top insets carry error bars that overlap zero, the drag-driven component of any apparent L/D improvement is correspondingly uncertain; apparent improvements in this region cannot be reliably decomposed into contributions from drag reduction versus lift enhancement. Meaningful interpretation of the percentage L/D improvement is therefore restricted to angles of approximately 5−20°, where the drag signal is more clearly resolved. At the peak L/D angle of 7°, where both the drag reduction signal and the L/D ratio are well-resolved, it is important to assess whether the observed improvements are attributable entirely to drag reduction or reflect an additional contribution from lift enhancement. Since SLIPS primarily reduces skin friction drag and friction drag constitutes a smaller fraction of total drag at nonzero angles of attack, the percentage drag reduction at 7° is

https://doi.org/10.1021/acs.chemmater.6c01113
Chem. Mater. XXXX, XXX, XXX−XXX

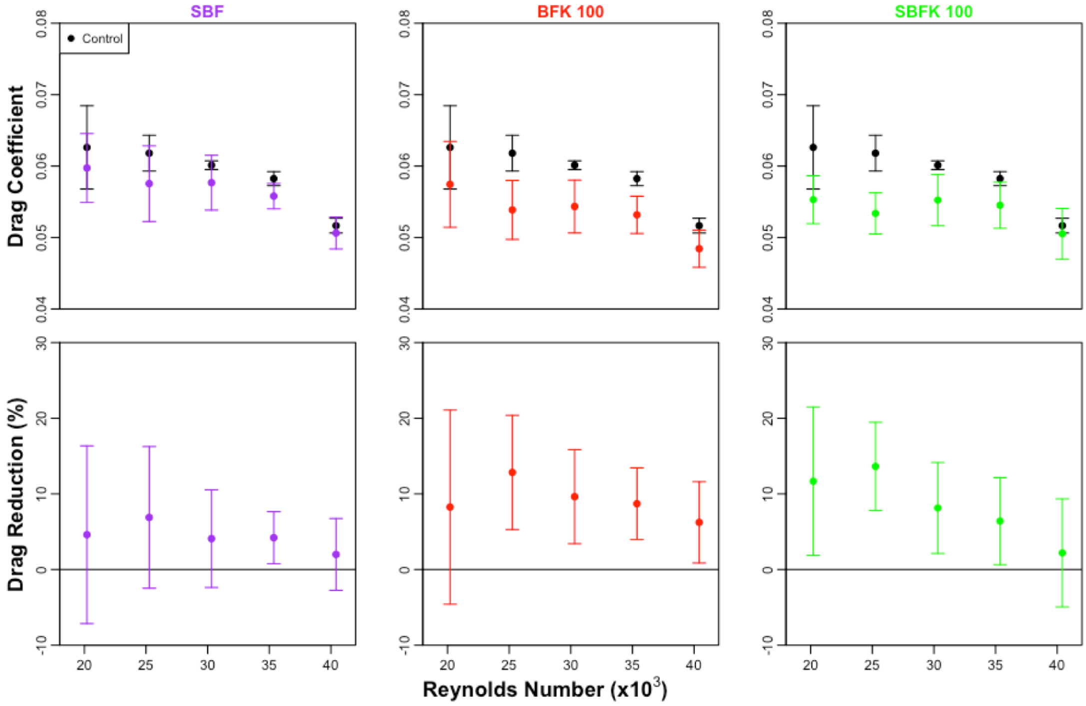

Figure 3. Static drag coefficient and drag reduction for coated and uncoated aluminum plates aligned parallel to the free-stream flow at zero angle of attack. *(Top)* Drag coefficient as a function of Reynolds number (Re) for the uncoated control (black), superhydrophobic SBF (purple), nanotextured SLIPS BFK 100 (red), and hierarchically textured SLIPS SBFK 100 (green) plates. Error bars represent ± one standard error ($N = 5$); error bars may be smaller than the symbols. *(Bottom)* Drag reduction (%) relative to the uncoated control for each coated surface. Error bars represent propagated standard errors computed from the standard errors of the paired coated and control drag measurements at each Reynolds number. Reynolds number is calculated based on the chord length of the plate.

Table 1. Summary of Hydrodynamic Performance Improvements for All Coated Surfaces Relative to the Uncoated Aluminum Control[a]

Plate Name	Static Drag Reduction (%) at 0° angle of attack	Increase in Max Lift/Drag (%)	Average Increase in Thrust (%)	Average Increase in Efficiency (%)
BFK 100	9.1 ± 3.5	4.3 ± 0.8	3.6 ± 0.8	4.1 ± 0.8
BFK 103	n/a	6.7 ± 0.8	1.2 ± 1.1	1.9 ± 1.1
SBFK 100	8.4 ± 3.2	8.7 ± 0.8	3.1 ± 1.3	3.2 ± 1.3
SBFK 103	n/a	7.6 ± 1.0	1.1 ± 0.2	1.3 ± 1.1
SBF	4.4 ± 3.5	n/a	n/a	n/a

[a]Static drag reduction (%) is averaged across all tested Reynolds numbers (Re = 20,000−40,000) at 0° angle of attack (Figure 3). The increase in maximum lift/drag ratio (%) is calculated at the peak lift/drag angle of attack (~7°) at 0.25 m/s (Figure 4). The average increase in thrust (%) and the average increase in propulsive efficiency (%) are averaged across all Strouhal numbers and pitch angles tested during dynamic flapping propulsion (Figures 5 and 6). The SBF surface is superhydrophobic but not lubricant-infused and was not tested under all conditions; BFK and SBFK surfaces are SLIPS-coated with Krytox 100 or Krytox 103 lubricant. Labels of n/a indicate that the test was not performed for that surface configuration.

expected to be lower than observed at 0° (Figure 3). For SBFK 100, the observed L/D improvement at 7° (8.7 ± 0.8%) approaches the 0° drag reduction (8.4 ± 3.2%), and since friction drag constitutes a smaller fraction of total drag at 7° than at 0°, the expected drag-reduction-driven L/D improvement at 7° would be lower still, suggesting that drag reduction alone may be an insufficient explanation and that a contribution from lift enhancement cannot be excluded. For BFK 100, where the L/D improvement (4.3 ± 0.8%) is substantially less than the 0° drag reduction (9.1 ± 3.5%), the data are consistent with a drag-reduction-only explanation. For BFK 103 and SBFK 103, the absence of 0° static drag data prevents this comparison from being made.

The effects of SLIPS coatings on thrust coefficient and propulsive efficiency during biomimetic flapping propulsion are shown in Figures 5 and 6. Flapping propulsion performance surfaces show a general increase in thrust coefficient with increasing Strouhal number (*St*), calculated as the product of flapping frequency and the peak-to-peak heave amplitude of the plate divided by the flow velocity,[54,55] with peak thrust occurring at a maximum pitch angle of 30° (Figure 5). The corresponding efficiency surface plots show an increase in efficiency with *St* up to a peak at $St = 0.4$ and a maximum pitch angle of 15° (Figure 6). The SLIPS-coated plates with lower-viscosity lubricant exhibit a modest but consistent average increase in both thrust and efficiency across the tested conditions (Table 1). The best-performing surface was the nanotextured BFK 100, which achieved an average thrust increase of 3.6 (±0.8)% (Figure 5A), followed by the hierarchically textured SBFK 100 plate with an average thrust increase of 3.1 (±1.3)% (Figure 5C). Comparable trends were observed in the efficiency data, with the BFK 100 plate increasing propulsive efficiency by 4.1 (±0.8)% (Figure 6A) and the SBFK 100 plate by 3.2 (±1.3)% (Figure 6C).

Lubricant viscosity also affects surface performance. BFK and SBFK plates were tested with two lubricants of differing dynamic viscosities, Krytox 100 and Krytox 103. Table 1 summarizes the percentage improvements in each performance metric for all

https://doi.org/10.1021/acs.chemmater.6c01113
Chem. Mater. XXXX, XXX, XXX−XXX

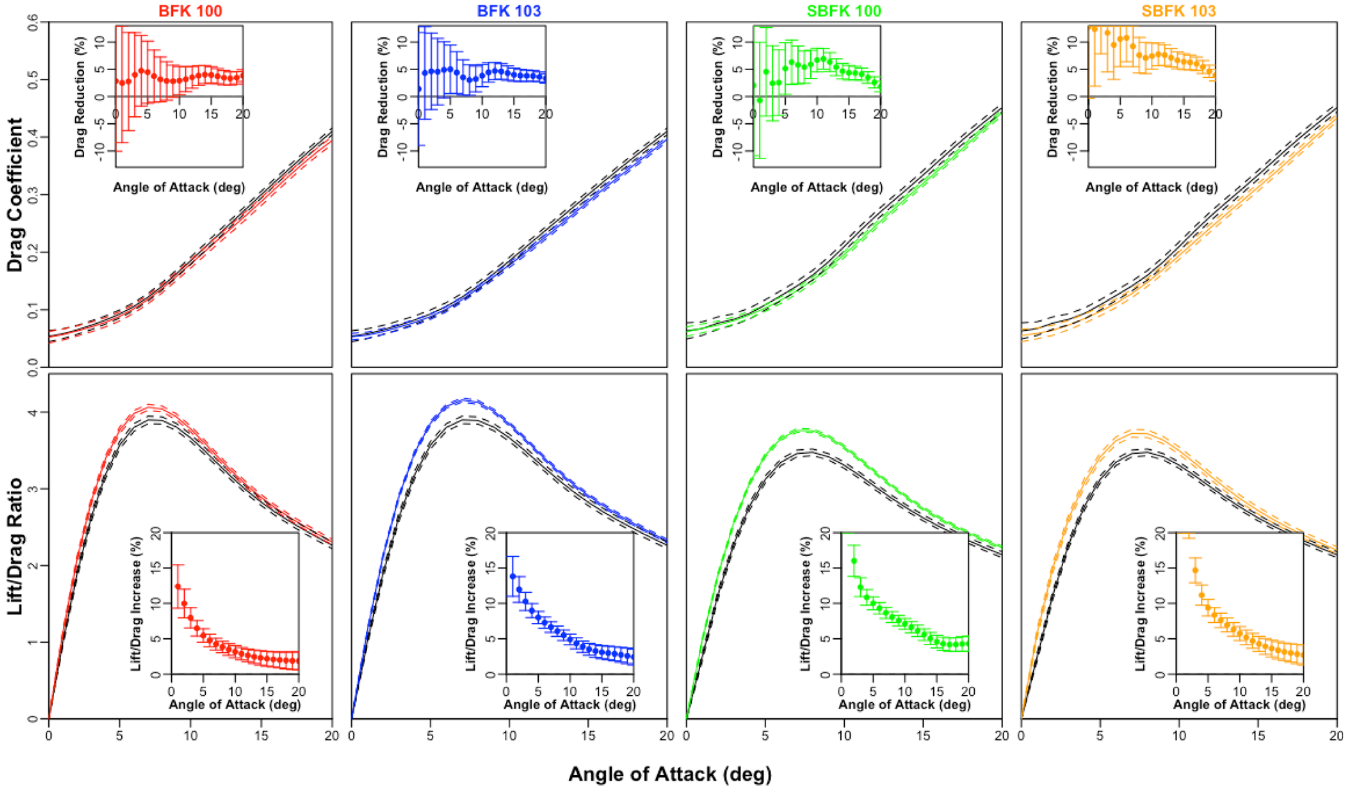

Figure 4. Drag coefficient and lift/drag ratio as a function of angle of attack for all four SLIPS-coated surfaces compared with the uncoated control at a free-stream velocity of 0.25 m/s. *(Top row)* Drag coefficient vs angle of attack for BFK 100 (red), BFK 103 (blue), SBFK 100 (green), and SBFK 103 (orange); the uncoated control is shown in black in each panel. *(Bottom row)* Lift/drag ratio vs angle of attack for the same surfaces. In all panels, the solid-colored curve shows a polynomial fit to the coated plate data, the solid black curve shows the polynomial fit to the control, and dashed lines show 95% confidence intervals. Insets show the percentage drag reduction (top row) and percentage lift/drag increase (bottom row) of each coated surface relative to the control, as a function of angle of attack up to 20°, beyond which substantial flow separation was observed. All four SLIPS achieve a peak lift/drag ratio near a 7° angle of attack, exceeding the control by between 4.3% and 8.7%. Forces were measured at 1° angle of attack increments, with five replicated trials (N = 5) at each angle. Error bars in insets represent propagated standard errors on the derived drag reduction and L/D improvement percentages.

surface types tested. For plates with identical surface textures but different lubricant viscosities, those infused with the lower-viscosity lubricant (Krytox 100) outperformed those infused with the higher-viscosity lubricant (Krytox 103) in five of the six cases reported. When comparing nanotextured BFK and hierarchically textured SBFK plates infused with the same lubricant, the nanotextured surface showed higher mean performance in five of the seven cases reported, though the differences were generally within the propagated standard errors; the exception was the increase in maximum L/D, where SBFK 100 clearly outperformed BFK 100 (8.7 ± 0.8% vs 4.3 ± 0.8%).

Using boundary layer particle tracking velocimetry (PTV), in which individual seeding particles are tracked across successive image frames to reconstruct near-wall velocity profiles, it was shown that SLIPS coating reduces wall shear stress through a change in the slope of the velocity gradient at the surface of a knife-edged plate under laminar flow conditions (Figure 7). The total shear stress was estimated by computing the trapezoidal Riemann sum of the shear stress distribution along the length of the knife-edged plates, allowing comparison between the nanotextured BFK 100 and the uncoated control plate. Wall shear stress on the SLIPS-coated plate ranged from 0.05 to 0.55 Pa across the tested flow velocities, representing an average reduction in shear stress of 5.2% relative to the uncoated aluminum surface. The reduction in near-wall velocity gradient and the corresponding increase in boundary layer thickness observed on SLIPS-coated surfaces are consistent with the introduction of an effective slip length at the lubricant-water interface. At the higher tested flow speed of 0.3 m/s, no measurable difference in wall shear stress was detected between the SLIPS-coated and control plates (Figure S2), a result consistent with the decrease in drag reduction observed at higher Reynolds numbers during static testing (Figure 3) and likely reflecting increased shear-driven lubricant drainage at higher flow speeds.

■ DISCUSSION

Does having a nanostructured slippery body surface enhance aquatic propulsion? Many aquatic vertebrates such as fish are covered with a mucus coating, retained in and on a rough surface, which has been proposed, among other functions, to reduce drag and thus enhance propulsion through the dense and viscous aquatic medium,[6,13,18,19] but experimental demonstration of the effectiveness of lubricants for swimming propulsion is lacking. The caudal fin of swimming fishes undergoes angular (pitch) and side-to-side (heave) motions during a tail beat cycle,[55−57] and the effectiveness of a lubricated surface relative to a smooth control surface undergoing such movement patterns is unknown. In addition, fish scales possess numerous micro-structural features that could act to hold a mucus lubricant on the surface,[18−20] suggesting that maintaining a mucus-like

https://doi.org/10.1021/acs.chemmater.6c01113
Chem. Mater. XXXX, XXX, XXX−XXX

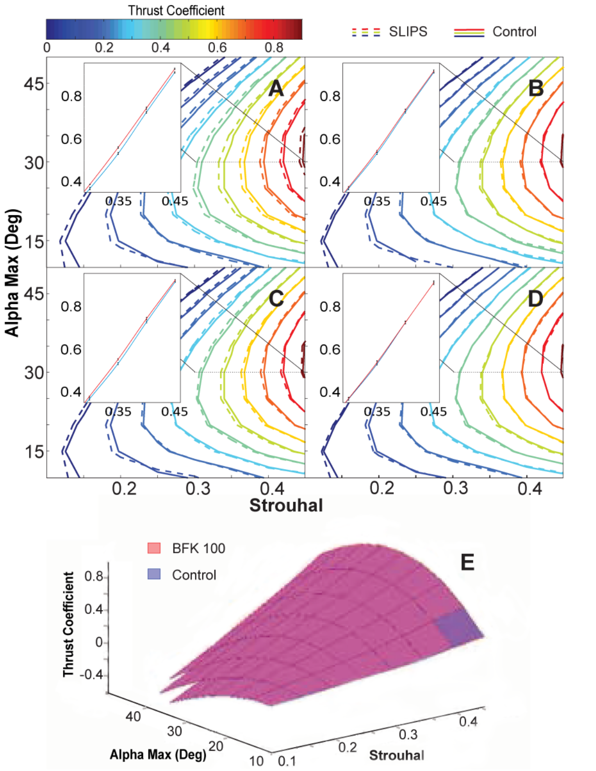

Figure 5. Thrust coefficient as a function of Strouhal number and maximum pitch angle (Alpha Max) during biomimetic flapping propulsion for all four SLIPS : (A) BFK 100, (B) BFK 103, (C) SBFK 100, and (D) SBFK 103. In each panel, contour lines represent constant thrust coefficient values (color scale: 0 to 0.9), with solid lines denoting the uncoated control and dashed lines denoting the SLIPS-coated surface. A consistent outward shift of the SLIPS contours relative to the control indicates higher thrust across the parameter space. Data points were collected at Strouhal number intervals of 0.05 and Alpha Max intervals of 5°, with each point averaged over five replicated trials ($N = 5$). Insets show cross-sections through the high-thrust region ($St = 0.30-0.45$), with the control shown as a blue curve and the SLIPS as a red curve; error bars represent ± one standard error. (E) Three-dimensional thrust coefficient surface plot for the BFK 100 treatment (red) overlaid with the uncoated control (blue), illustrating the broad elevation in thrust across the full parameter space imparted by the SLIPS coating.

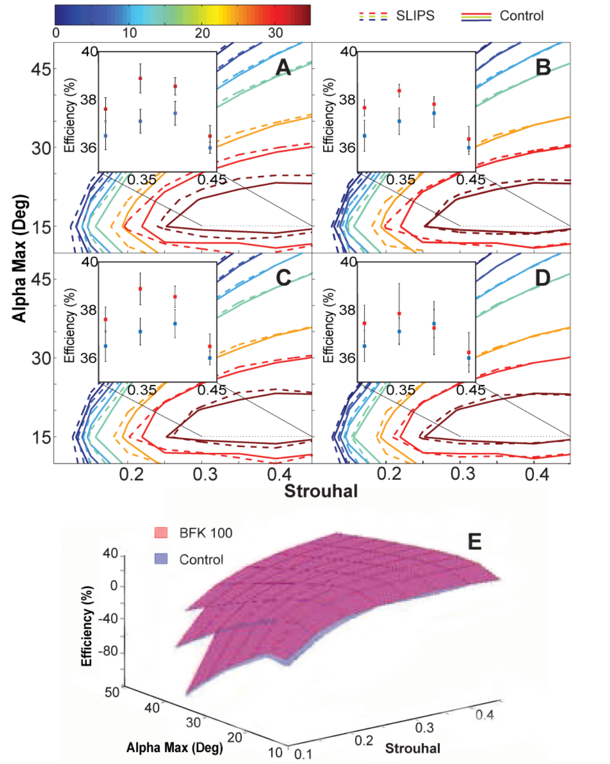

Figure 6. Propulsive efficiency as a function of Strouhal number and maximum pitch angle (Alpha Max) during biomimetic flapping propulsion for all four SLIPS: (A) BFK 100, (B) BFK 103, (C) SBFK 100, and (D) SBFK 103. In each panel, contour lines represent constant propulsive efficiency values (color scale: 0 to 35%), with solid lines denoting the uncoated control and dashed lines denoting the SLIPS-coated surface. A consistent outward shift of the SLIPS contours relative to the control indicates higher propulsive efficiency across the parameter space, with peak efficiency occurring near $St = 0.4$ and Alpha Max = 15°. Data points were collected at Strouhal number intervals of 0.05 and Alpha Max intervals of 5°, with each point averaged over five replicated trials ($N = 5$). Insets show absolute propulsive efficiency values in the high-efficiency region ($St = 0.30-0.45$), with the SLIPS (red squares) consistently exceeding the control (blue squares); error bars represent ± one standard error. (E) Three-dimensional propulsive efficiency surface plot for the BFK 100 treatment (red) overlaid with the uncoated control (blue), illustrating the broad increase in efficiency conferred by the SLIPS coating across the full parameter space. Negative efficiency values at low Strouhal numbers reflect conditions under which the power input exceeds thrust output.

lubricated coating could be important for enhancing propulsion. Experiments on how mucus affects propulsion in freely swimming animals are difficult to accomplish, as approaches involving the removal of mucus and subsequent comparison with unmodified animals are unlikely to be effective because of the many uncontrolled factors involved. A controlled mechanical model for propulsion[58,59] represents a useful tool for analyzing how different slippery surfaces could affect aquatic propulsion and for quantitatively determining the magnitude of the effect that a slippery propulsive surface can have on both thrust and efficiency.

The effects of one superhydrophobic surface (SBF) and two biomimetic mucus-like lubricated SLIPS (BFK and SBFK; Figure 1) on drag and propulsion were examined at *Re* values that approximate those experienced by swimming fishes of moderate size (20−30 cm in total length) at speeds corresponding to routine swimming of approximately one body length per second. Fabricated textured surfaces were employed to retain lubricants on the surface (Figure 1), using lubricants of similar average viscosity to measured trout mucus (Figure 2) under conditions of shear stress comparable to those experienced by swimming fishes (Figure S3). Shear stresses on the surface of freely swimming trout have been measured between 0.05 and 0.4 Pa (depending on the phase of body motion),[60] a range comparable to the shear stress values measured on the flat plates (Figures 7, S2) in the present experiments. Furthermore, the ability to control and isolate different properties of the surfaces tested allowed for the examination of the effects of both lubricant viscosity and surface roughness relative to a smooth control.

The SLIPS-coated surfaces produced greater static drag reduction than the superhydrophobic surface at a 0° angle of attack (Table 1); the superhydrophobic surface was not tested under lift-to-drag ratio or dynamic propulsion conditions, so the comparison between surface types is limited to the static drag result. This result warrants further explanation, as it is

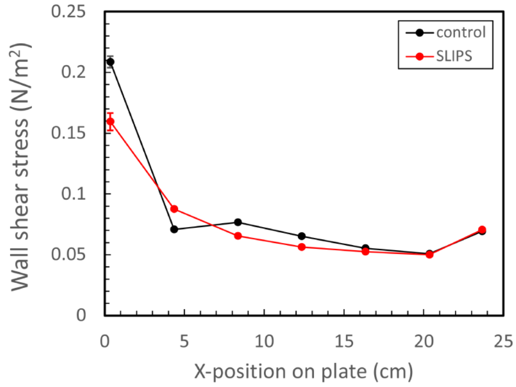

Figure 7. Wall shear stress along the streamwise length of the knife-edged flat plate at a free-stream flow velocity of 0.15 m/s, measured by particle tracking velocimetry. Shear stress is shown at seven positions from the leading edge for the nanotextured SLIPS-coated plate (BFK 100, red) and the smooth uncoated control (black). Both surfaces exhibit decreasing wall shear stress with increasing downstream distance, consistent with the development of a laminar boundary layer. The SLIPS-coated plate shows consistently lower wall shear stress than the control, particularly near the leading edge, representing an average reduction of 5.2% integrated along the plate length. Error bars represent ± one standard error ($N = 400$ velocity profiles per position).

counterintuitive under the classical apparent-slip model: with $\mu_{water}/\mu_{air} \approx 55$ versus $\mu_{water}/\mu_{Krytox100} \approx 0.05$, the model predicts that a surface trapping air should generate slip lengths and drag reduction roughly 3 orders of magnitude larger than one infused with PFPE lubricant for equivalent layer thicknesses. The observation that SLIPS outperforms the superhydrophobic SBF surface therefore reflects not a failure of the apparent-slip model per se, but a fundamental difference in interfacial retention under the macroscale turbulent flow conditions of our experiments (Re = 20,000−40,000). On the SBF surface, drag reduction arises from a partial slip condition at an air−water interface trapped within the surface texture;[61] however, such air pockets are susceptible to pressure-driven collapse and displacement by water penetrating the texture via a Cassie-to-Wenzel transition, particularly under the elevated shear stresses of flow testing.[62−64] On the SLIPS, by contrast, the immiscible PFPE lubricant is stabilized within the texture by chemical affinity between the fluorinated phosphoric acid functionalization layer and the perfluoropolyether lubricant, providing a thermodynamically favorable and mechanically robust lubricated interface that is maintained under shear. The superior drag reduction of SLIPS over the superhydrophobic surface thus reflects not simply a viscosity effect, but a more stable interfacial chemistry that sustains the slip condition throughout testing. The measured drag reduction on the SBF surface therefore represents an average over a surface that progressively transitions from superhydrophobic to partially wetted during testing, rather than a steady-state measurement on an intact plastron, explaining the apparent underperformance relative to model predictions. Lubricant thickness data collected before and after the experiments provide insight into how roughness and lubricant thickness affect drag reduction (Table S1). Prior to flow tank testing, the lubricant layer on the hierarchically textured SBFK plates was greater in thickness than on the nanoscale textured BFK plates (Table S1). After removal of the hierarchical plates from the flow tank, the lubricant layer retained on them remained greater than the average surface roughness (Table S1), although some microscale surface features may have protruded through the lubricant layer, potentially diminishing the drag-reducing capability of the surface. Despite surface texturing, some lubricant loss occurred during testing, although the higher-viscosity lubricant (Krytox 103) showed a lower percentage loss than the lower-viscosity lubricant (Krytox 100). The observation that the higher-viscosity lubricant exhibited lower percentage loss during testing is consistent with previously published models of lubricant consumption dynamics, which concluded that lubricant escape rate is strongly influenced by the viscosity contrast between the infusing fluid and the external flow, with higher-viscosity lubricants resisting shear-driven drainage more effectively.[39,65] For the nanoscale textured plates, the lubricant layer was thinner than that of the hierarchical plates; however, this thickness was an order of magnitude greater than the height of nanoscale texturing (typically 100−200 nm) such that none of the surface features were likely to protrude through the lubricant layer. These results are consistent with lubricant thickness observations from contact angle hysteresis monitoring of water on SLIPS subjected to increasing shear stress.[40] A further key aspect of performance is the dependence on the viscosity ratio of the external liquid (water) to that of the infusing lubricant (μ_{water}/μ_{oil}), with higher ratios of $\mu_{water}/\mu_{oil} \sim 0.25$ associated with better performance, consistent with prior experimental and theoretical results.[36−38,66] The superior thrust and propulsive efficiency improvements for lower-viscosity Krytox 100 relative to higher-viscosity Krytox 103 are consistent with the finding that mucus viscosity is positively correlated with interface stability but negatively correlated with drag reduction rate, with higher viscosity stabilizing the lubricant-water interface but simultaneously increasing interfacial shear stress, with the net effect being reduced drag reduction efficiency at higher viscosities.[35,67]

Recent microfluidic studies have identified an additional mechanism contributing to slip on lubricant-infused surfaces beyond the viscosity-ratio (apparent-slip) model: the spontaneous nucleation of surface nanobubbles on regions of the underlying hydrophobic substrate exposed by local lubricant depletion. Using AFM meniscus-force mapping on silicone oil-infused Teflon nanowrinkled surfaces, Vega-Sánchez et al. showed that effective slip lengths up to 50 times larger than apparent-slip predictions are attributable to nanobubbles with low protrusion angles that nucleate at dewetted surface regions.[68] Detection of these features using AFM revealed the coexistence of oil-covered, nanobubble-covered, and bare substrate regions on the immersed liquid-infused surfaces.[69] Subsequent work showed that the lubricant layer stabilizes nanobubbles against pressure-induced dissolution relative to dry superhydrophobic surfaces[70] and that bubble nucleation is a general phenomenon for rough hydrophobic lubricant-infused surfaces regardless of surface-lubricant spreading compatibility, occurring once sufficient lubricant depletion exposes the substrate.[71] Molecular dynamics simulations have further established that nanobubble protrusion angle, coverage, and fluidity collectively control the sign and magnitude of the slip length.[72] These results were obtained under laminar, microfluidic conditions on nanostructured surfaces; their quantitative applicability to the macroscale turbulent-flow regime studied here remains an open question. Nevertheless, they indicate that lubricant viscosity plays multiple coupled roles: it directly sets the apparent-slip contribution at oil-covered regions through the viscosity ratio (μ_{water}/μ_{oil}); it controls the rate of shear-driven lubricant depletion that determines the density of hydrophobic sites available for bubble nucleation; and it modulates the

https://doi.org/10.1021/acs.chemmater.6c01113
Chem. Mater. XXXX, XXX, XXX−XXX

stability of any nucleated gas phase through the lubricant cloaking layer. The superior drag reduction and propulsive performance of the lower-viscosity Krytox 100 surfaces relative to Krytox 103 is consistent with all three of these mechanisms operating in concert. Looking forward, these insights suggest that lubricant chemistry itself represents an underexplored design lever: selecting lubricants with intrinsically high gas solubility, such as the perfluorinated compound 1-bromoheptadecafluorooctane recently employed by Park and Lee,[73] can actively promote interfacial gas layer formation under photothermal irradiation and enhance drag reduction beyond what viscosity ratio or passive nanobubble nucleation alone would produce, representing a promising direction for the next generation of mucus-inspired lubricated surfaces for marine applications.

Fish scales commonly bear hierarchical surface features spanning multiple length scales, such as concentric circuli and ctenoid spines, and it has been proposed that this multiscale surface microroughness aids in anchoring the mucus and epidermal layer against shear-driven removal during swimming, an indirect hydrodynamic function distinct from direct flow modification.[4] Quantitative profilometry across seven species shows that mucus reduces surface roughness by 40−93% in most fishes, consistent with mucus filling and smoothing scale microfeatures in a manner analogous to lubricant infilling the textured surfaces of the SBFK plates. Some of these microscale features protrude through the mucus layer, although the extent to which this occurs varies considerably among species.[18,19] Analysis of fish surface roughness with and without the natural mucus coating shows that some species, such as Brook trout (*Salvelinus fontinalis*), have scales almost completely covered by mucus, creating a smooth surface with a maximum feature height of 7 μm, while other species, such as the Niger triggerfish (*Odonus niger*), have scales that protrude to as much as 200 μm above the surface when the mucus coating is intact.[4] Brook trout, in particular, exhibit a mucus coating that nearly completely covers all scale surface features, yielding an extremely smooth body surface with an average roughness of 0.6 μm, compared to 8.6 μm when the mucus is removed.[4] Another biological parallel is found in the puffer fish (*Takifugu obscurus*), where it has been shown that surface spines can anchor the outermost mucus layer against shear-driven washout at high flow velocities.[12]

One aspect of the fish mucus coating that is not replicated in the present experimental system is its renewable nature. Fish skin possesses a large number of goblet cells that continuously renew the mucus coating, thereby refreshing the lubricated surface over time.[74] Some lubricant loss was observed during the experiments despite the surface texturing, and it is likely that fish experience analogous sloughing of mucus, which is subsequently replaced as a result of body deformation and water flow over the body during swimming.[75]

Reported measurements of fish mucus indicated that mucus viscosity was highly dependent on the water content within the sample.[6,12,14] This characteristic was also observed in the mucus collected from *Salvelinus fontinalis* (Figure 2), as even the as-collected mucus samples exhibited a viscosity nearly four times greater than that of water over the entire range of shear rates tested. When the low-viscosity aqueous component of mucus was removed by centrifugation, fish mucus exhibited a strong shear-rate dependence. The range of shear rates tested encompasses values estimated for the surface of swimming fishes,[8] and it is therefore expected that the drag reduction, improvement in the lift-to-drag ratio, reduction in shear stress, and increases in thrust and efficiency observed for the SLIPS-coated aluminum plates could correspond to analogous improvements in the locomotor dynamics of freely swimming fish. The shear-thinning behavior exhibited by dewatered trout mucus at higher shear rates may confer additional propulsive benefits beyond those captured by the Newtonian perfluoropolyether lubricants used in the present study, as numerical simulations indicate that shear-thinning fluids on surfaces can reduce drag and hydrodynamic power consumption relative to Newtonian fluids of equivalent viscosity.[11,76] Rheological characterization of puffer epidermal mucus demonstrates this mechanism directly: under increasing shear, the apparent viscosity of mucus decreases progressively, breaking down the mucin chain entanglement and forming a slip condition at the mucus-water interface that reduces frictional drag.[12] Unlike Newtonian lubricants, which maintain constant viscosity under shear, biological mucus can become more effective as an interfacial lubricant precisely under the high-shear conditions of active swimming. An important caveat is that shear-thinning behavior is expected to present a retention trade-off. While decreasing the viscosity under shear promotes slip and drag reduction, it may simultaneously reduce the cohesive integrity of the interfacial layer and accelerate its removal at higher speeds. Quantifying this trade-off between rheological drag reduction and coating durability represents a key challenge for the development of next-generation mucus-inspired surfaces. It should also be noted that fish mucus is a viscoelastic material, displaying elastic storage and viscous loss moduli characteristic of a gel-like mucin network, in addition to shear-thinning steady-shear viscosity; the Newtonian PFPE lubricants used here do not replicate this viscoelastic character. The present study is designed to isolate the effect of viscosity ratio on interfacial drag reduction as a necessary mechanistic baseline; as shown in Figure 2, as-collected hydrated trout mucus displays approximately Newtonian behavior in the shear rate range most representative of steady-swimming conditions. Fully replicating the rheological complexity of in vivo mucus, including its elastic component, would require future experiments with viscoelastic interfacial coatings, such as mucin-functionalized or hydrogel-brush surfaces.

The most striking result of this study is the broad parameter space over which improvements in both thrust and efficiency were observed during flapping (dynamic) propulsion for surfaces infused with the lower-viscosity lubricant (Krytox 100). The *a priori* expectation was that a slippery surface coating might enhance propulsion only under certain movement parameters, perhaps over a limited range of Strouhal Numbers (*St*) or at particular values of plate heave or pitch. However, a slippery coating was found to confer a broad performance advantage (Figures 5, 6), with improvements in both thrust and efficiency of approximately 3−4% obtained across essentially all motion parameters used to drive propulsion for the lower-viscosity-infused surfaces. These improvements during dynamic testing can be understood as a consequence of the improvements in the lift-to-drag ratio observed during static testing (Figure 4; Supplemental Movie S1). The lift-to-drag improvement itself arises primarily from the reduction in skin friction drag at nonzero angles of attack, with a possible contribution from lift enhancement for some surfaces, as assessed by comparison of the drag reduction and L/D improvement insets in Figure 4. It is important to note that the two components of the static performance data differ in their statistical robustness. The drag reduction values at 0° angle of attack carry substantial

https://doi.org/10.1021/acs.chemmater.6c01113
Chem. Mater. XXXX, XXX, XXX−XXX

propagated measurement uncertainties (Figure 3, bottom row), and the evidence for drag reduction rests on the consistent positive trend observed across all tested Reynolds numbers and surface types rather than on the statistical robustness of the individual data points. The L/D improvement data present a stronger statistical picture: near the peak L/D angle of 7°, where the separation between the coated and control polynomial fits is greatest, the improvements for all four SLIPS are clearly distinguishable from zero (Figure 4, bottom row insets), representing the most statistically supported finding in the static testing component of this study. The increase in thrust observed is hypothesized to result in part from modifications to flow separation patterns and leading-edge vortex (LEV) dynamics over the flapping aluminum plates, though direct flow visualization of this effect in the context of SLIPS-coated surfaces remains an important direction for future work. An analogous LEV effect was documented for shark skin,[77] showing that changes in the surface roughness of shark skin altered LEV position in a manner consistent with improved swimming performance due to increased leading-edge suction. Given that propulsive efficiency improvements of up to 4.1% were observed consistently across a broad range of motion parameters, the energetic savings for a fish sustaining continuous swimming over extended periods could be biologically substantial, with potential consequences for foraging range, predator escape performance, and migratory capacity.

Although the locomotor literature has naturally focused on drag reduction by textured and coated surfaces, it is important to emphasize that slippery coatings can also enhance thrust, as shown here, and that proposed mechanisms of performance improvement attributable to surface texture should also consider effects on thrust generation. Thrust enhancement further results in increased propulsive efficiency, indicating that less energy is consumed to move through water with a slippery-coated surface. The simultaneous enhancement of thrust and reduction of drag observed for SLIPS-coated plates is qualitatively consistent with numerical simulations of undulatory foils with shear-thinning mucus-like fluid interfaces, which predict that a slippery boundary layer coating reduces friction drag while also enhancing net thrust production and reducing force oscillations during the swimming stroke,[11] although it is noted that the Newtonian perfluoropolyether lubricants used in the present study produce drag reduction through a Navier slip mechanism rather than through non-Newtonian shear-thinning effects.

Previous boundary-layer flow visualization experiments on fresh fish skin suggested that fish mucus reduces wall shear stress through a change in the velocity gradient within the boundary layer,[6,13] an effect qualitatively consistent with the boundary-layer modifications observed here on SLIPS-coated surfaces (Figure 7). This supports the hypothesis that both fish mucus and SLIPS produce drag reduction through a common underlying mechanism: the lubricant fills surface texture features, introducing an effective slip length at the lubricant-water interface and reducing the near-wall shear stress. Slip length, defined as the effective distance projected onto the solid surface at which the linear extension of the wall velocity gradient satisfies the no-slip condition,[78] provides a unifying framework for understanding drag reduction on both biological and engineered lubricated surfaces. More precisely, the drag reduction observed here is consistent with apparent slip rather than true molecular slip at the solid surface: the immiscible PFPE lubricant layer acts as a lower-viscosity interfacial fluid, shifting the effective slip plane from the solid−water interface to the lubricant-water interface and producing a measurable reduction in the near-wall velocity gradient.[79] This distinction is important because apparent slip arising from a viscosity-mismatched fluid interface is mechanistically distinct from the molecular-level sliding proposed for true slip and is the physically appropriate description for lubricant-infused surfaces where a continuous low-viscosity phase is maintained at the wall. The reduction in near-wall velocity gradient and increase in boundary layer thickness observed here are further consistent with boundary-layer modifications reported for bioinspired mucus-releasing surfaces,[16] suggesting a shared mechanism. In swimming fish, where mucus covers many scale surface features,[4] an analogous reduction in wall shear stress could contribute meaningfully to locomotor economy.

■ CONCLUSION

By using flapping plates as a simplified mechanical model of aquatic locomotion, coating these plates with a liquid-infused SLIPS of viscosity similar to that of fish mucus, and directly measuring both drag forces, propulsive thrust, and efficiency, the present study provides experimental evidence that slippery surface coatings impart measurable hydrodynamic benefits under both static and dynamic conditions. These results address a longstanding question in the biology of aquatic locomotion: whether the mucus coating found on a diversity of fish and other aquatic vertebrates provides a functional benefit for swimming.

Under static conditions, SLIPS-coated surfaces reduced drag by up to 9.1%, consistent with a positive drag reduction trend across all tested conditions, and enhanced the lift-to-drag ratio by up to 8.7% relative to the uncoated control, with boundary layer measurements confirming a corresponding reduction in near-wall shear stress of up to 5.2%. This is consistent with the introduction of an effective slip length at the lubricant−water interface, which is qualitatively analogous to the boundary layer modifications previously attributed to fish mucus.

Under dynamic propulsive conditions, lower-viscosity SLIPS coatings improved the thrust by up to 3.6% and the propulsive efficiency by up to 4.1%, with gains observed consistently across the full range of Strouhal numbers and pitch angles tested. The broad distribution of these improvements across the motion parameter space suggests that a slippery coating provides a robust propulsive advantage and that drag reduction alone is an incomplete characterization of the locomotor benefits of such surfaces.

Several important limitations of the present study should be considered for future work. The plates tested here were rigid, whereas the bodies and fins of swimming fish are flexible and undergo continuous undulatory deformation. Although the Strouhal numbers and Reynolds numbers employed span values relevant to the routine swimming of moderate-sized fish, the full complexity of undulatory propulsion was not captured. Furthermore, the perfluoropolyether lubricants used are Newtonian fluids, whereas biological fish mucus exhibits shear-thinning behavior at higher shear rates. Numerical simulations suggest that shear-thinning interfaces may confer additional propulsive benefits beyond those produced by Newtonian lubricants of equivalent viscosity, implying that the improvements measured here may represent a conservative lower bound on the performance gains achievable with a biologically realistic mucus analog. Advances in SLIPS coatings that enable application to flexible and elastomeric substrates now provide an opportunity to test these effects under more realistic undulatory propulsion conditions and to more directly model

https://doi.org/10.1021/acs.chemmater.6c01113
Chem. Mater. XXXX, XXX, XXX−XXX

the continuous mucus renewal that occurs at the surfaces of living fishes.

Together, these findings demonstrate that reductions in friction drag, enhancement of the lift-to-drag ratio, and improvements in propulsive thrust act as complementary mechanisms by which slippery coatings improve the overall efficiency of fish-like locomotion. The broad and consistent nature of the performance improvements measured across surface types and motion parameters supports the hypothesis that the mucus coatings of aquatic vertebrates provide a genuine locomotor advantage and offer a biologically grounded rationale for the widespread presence of such coatings across a diversity of species. The energetic savings associated with efficiency improvements of this magnitude, sustained over long-duration or high-frequency swimming, could have meaningful consequences for ecologically critical behaviors, including foraging, predator evasion, and long-distance migration.

■ MATERIALS AND METHODS

Sample Preparation

All plates measured 190 mm × 68.5 mm × 3 mm (height × width × thickness) and were fabricated from 6061 aluminum alloy; a smooth, uncoated plate of the same material served as the control. The SLIPS coating process, adapted from Kim et al.,[40] is summarized in Figure 1. Hierarchical (SBF) plates were produced in three steps: sandblasting ("S"), boehmitization ("B"), and functionalization ("F"). Nanostructured (BF) plates were produced in two steps: boehmitization ("B") and functionalization ("F").

Sandblasting used 120-grit alumina (average particle diameter 125 μm), creating a microscale texture with an average roughness of 3.2 μm. Boehmite (aluminum oxyhydroxide, AlO(OH)) was formed by boiling the plates in distilled water for 10 min, producing a uniform nanoscale layer 10−30 nm thick. The resulting AlO(OH) surface is rich in hydroxyl groups, which serve as anchoring sites for the subsequent fluorinated functionalization step through coordinative ligand exchange. Surfaces were then functionalized by immersion in an ethanol bath containing 1 wt % Masurf FS-100 (phosphoric acid with mixed-length fluorinated alkyl chains) at 70 °C for 10 min, creating an affinity for the liquid perfluoropolyether (PFPE) lubricant, Krytox (DuPont Inc., Wilmington, DE, USA). The SBF and BF surfaces exhibited superhydrophobic properties following these treatments, as previously reported.[40]

Prior to flow tank testing, Krytox lubricant was applied to the entire SLIPS plate surface using a pipet; then, each plate was suspended vertically for 1 h to allow excess lubricant to drain. Two lubricants of differing viscosity were used: Krytox GPL 100 (K100; density = 1.835 g/mL, μ = 20 mPa·s at 25 °C) and Krytox GPL 103 (K103; density = 1.884 g/mL, μ = 120 mPa·s at 25 °C). The coating applied to each plate is summarized in Table S2.

The relationship between lubricant volume and surface feature height was confirmed by gravimetric measurements of each plate type in the dry state, after lubricant application, and after flow tank testing (Table S1). For the BFK nanoscale surfaces, the applied lubricant formed a layer an order of magnitude thicker than the boehmite nanostructure height (10−30 nm leaflet thickness; ∼100−200 nm overall texture), ensuring complete submersion of surface features. For the SBFK hierarchical surfaces, the estimated lubricant layer exceeded the average microscale roughness (3.2 μm) under both pre- and posttest conditions, consistent with lubricant infilling the texture. Contact angle hysteresis on identically prepared surfaces has been reported previously,[40] where lubricated nanotextured and hierarchical surfaces exhibited CAH values of 2.9 ± 1.6° and 3.6 ± 1.0°, respectively, confirming stable SLIPS formation.

Measurement of Fish Mucus and Lubricant Viscosity

Mucus was collected weekly over 5 weeks from five Brook trout (*Salvelinus fontinalis*) ranging in total length from 20 to 30 cm. All research on trout mucus was conducted under the animal care and use protocol IACUC 20-03-2 from Harvard University. Trout were maintained alive in the Lauder Laboratory at Harvard University, and mucus was collected once a week from several individual fish over the five week period. Fish were captured using a net, a small amount of mucus was scraped from their skin surface, and the fish were returned to their home tank alive. No mortality or adverse effects were observed in the years subsequent to this procedure. Mucus was stored at −20 °C between collection periods as sufficient sample volumes were accumulated for analysis. Trout were obtained from a fish hatchery in Massachusetts, USA, and were obtained and housed in accordance with all Harvard University IACUC protocol requirements.

Prior to rheological testing, the pooled mucus was centrifuged at 2000 rpm for 2 min to remove excess water. The viscosity of the resulting dense phase is reported as "Dewatered T.M.". Synthetic perfluoropolyether lubricants were tested without further processing. The steady-state flow viscosity of all materials was measured at 25 °C using a TA Instruments Discovery HR-3 rheometer, with a shear rate sweep from 10 s^{-1} to 200 s^{-1} performed in a cone-and-plate configuration using a 40 mm, 2° cone geometry. Viscosity measurements of trout mucus and Krytox lubricants were each repeated three times and reported as a mean value with standard error.

Experimental Apparatus

Hydrodynamic testing was conducted in a freshwater recirculating flow tank equipped with heave and pitch motors mounted above the working section. The flow tank had a rectangular cross-section of 0.25 m × 0.30 m and a 0.9 m working length, and it has been used previously for experiments on fish locomotion[80−82] and flapping foil propulsion.[59,83,84] Tunnel blockage was minimal, with the frontal area of the plate at 0° angle of attack constituting less than 1% of the channel cross-sectional area. Plates were mounted on an 8 mm stainless steel shaft and submerged at mid-depth (Supplemental Figure S1B), with an ATI Nano-17E six-axis force/torque transducer (ATI Industrial Automation Inc., USA) attached to the shaft to measure three forces (F_x, F_y, F_z) and three torques (T_x, T_y, T_z) simultaneously (Supplemental Figure S1A). The recirculating flow tank used for the experiments had a temperature control system that maintained the water temperature at 20 °C (±1 °C).

Static Testing

Static drag was measured with each plate centered in the tank and aligned parallel to the flow at six speeds between 0.30 and 0.59 m/s (0.074 m/s increments). The flow channel Reynolds number, Re_{ch}, calculated using flow velocity and channel width (0.25 m), ranged from 20,200 to 40,100, corresponding to the Re range of 20−30 cm fish swimming at routine speeds of approximately one body length per second. The flow tank hydraulic radius (6.8 cm) yields Re values nearly identical to those calculated using the plate chord length (6.85 cm). Each drag measurement was repeated five times (N = 5) over a 10-s sampling period at 1000 Hz, and the mean value with standard error is reported.

Lift and drag forces were measured at 1° angle-of-attack increments from 0° to 45° at a flow speed of 0.25 m/s, using a custom LabVIEW program (National Instruments, USA). Flow was allowed to settle for 30 s at each angle before recording data for 10 s at 1000 Hz. Reported values are the means from five replicated trials (N = 5) with standard error.

Drag coefficients and lift-to-drag ratios were fitted as a function of angle of attack using polynomial regression (20th-degree orthogonal polynomial for drag; 18th-degree polynomial forced through the origin for L/D). Standard errors of the polynomial fits were extracted by dividing the half-width of the 95% confidence interval from the fitted model by the corresponding t-value at the residual degrees of freedom. Percentage differences between coated and control surfaces were then computed from the fitted values at each angle, and standard errors on these percentage differences were propagated analytically using the standard formula for the ratio of two independent quantities:

https://doi.org/10.1021/acs.chemmater.6c01113
Chem. Mater. XXXX, XXX, XXX−XXX

$$SE_\Delta = \frac{100}{|\hat{y}_{ctrl}|}\sqrt{\left(\frac{\hat{y}_{treat}}{\hat{y}_{ctrl}}\right)^2 SE_{ctrl}^2 + SE_{treat}^2}$$

where $\hat{y}_{ctrl}$ and $\hat{y}_{treat}$ are the fitted values for the control and treatment surfaces respectively, and SE_{ctrl} and SE_{treat} are their associated standard errors. Error bars in figures represent ±1 propagated standard error.

Dynamic Testing

Plates were tested with sinusoidal heave and pitch motions, similar to the method used by Read et al.[55] The heave, $h(t)$, and pitch, $\theta(t)$, motions are defined as

$$h(t) = h_0 \sin(2\pi f t)$$

$$\theta(t) = \theta_0 \sin\left(2\pi f t + \frac{\pi}{2}\right)$$

All tests were carried out at a heave amplitude h_0 = 0.05 m and free-stream flow velocity U = 0.25 m/s. Tests were parametrized by Strouhal number (St) and maximum angle of attack, α_{max}. St is calculated as the product of flapping frequency and the peak-to-peak heave amplitude of the plate ($2h_0$) divided by flow velocity.[54] Data points were collected for St ranging from 0.1 to 0.45 in increments of 0.05 and α_{max} ranging from 10° to 50° at 5° intervals. The frequency for each data point is chosen based on St:

$$f = \frac{U \times St}{2h_0}$$

and the pitch amplitude is set based on the maximum angle of attack:

$$\theta_0 = -\arctan\left(\frac{\dot{h}(t)}{U}\right) + \alpha_{max}$$

For each St and α_{max} combination, 10 s of force, torque, heave, and pitch data were recorded at 1000 Hz and phase-averaged prior to computing thrust coefficient and efficiency. Mean thrust force, $\overline{F}_x$, and mean power used to drive the plate, $\overline{P}$, are computed over one phase-averaged cycle as

$$\overline{F}_x = \frac{1}{N}\sum_{i=1}^{N} F_x(t_i) \text{ and } \overline{P} = \frac{1}{N}\sum_{i=1}^{N}\left[F_y(t_i)\dot{h}(t_i) + Q(t_i)\dot{\theta}(t_i)\right]$$

where $t_i = i\Delta t$ are the sample times, Δt = 1 ms is the sampling interval, and $N = T/\Delta t$ is the number of samples in one flapping period $T = 1/f$. F_x is the instantaneous streamwise force; F_y is the instantaneous lateral force in the heave direction; and Q is the instantaneous pitch torque.

Thrust coefficient, C_T, and power coefficient, C_P, are calculated as

$$C_T = \frac{\overline{F}_x}{\frac{1}{2}\rho c s U^2} \text{ and } C_P = \frac{\overline{P}}{\frac{1}{2}\rho c s U^3}$$

Propulsive efficiency, discussed in Read et al.,[55] is given as

$$\eta = \frac{C_T}{C_P}$$

Table 1 reports mean percent increase in thrust and propulsive efficiency for each surface treatment relative to the uncoated control, averaged across 62 of 68 experimental conditions (8 Strouhal numbers × 9 maximum pitch angles, with 4 conditions absent from all treatments) after applying a 5% trimmed mean (3 conditions removed from each tail of the percent difference distribution, 8.8% of conditions in total). Percent differences were computed for each condition by comparing condition-level means calculated from N = 5 replicates. Uncertainty represents the propagated standard error of the trimmed mean. A summary of all tests performed on each plate is provided in Supplementary Table S2.

Knife-Edge Flat Plate Boundary Layer Experiments

Flat plates measuring 25 cm in streamwise length and 50 cm in width were fabricated from 3/16-in. aluminum sheet, with leading edges beveled at 10° on the rear face to form a knife-edge profile suitable for boundary layer measurements. The SLIPS plate (BFK 100) was subjected to boehmitization and functionalization and then lubricated with Krytox 100 prior to testing. The control plate was left as bare aluminum. During testing, each plate was clamped to a beam parallel to the flow, centered above the flow tank, and oriented vertically to span from the bottom of the flume to the free surface. A 5 W continuous-beam argon-ion laser (Coherent I310) was positioned to illuminate the front face of the plate 10.2 cm above the tank floor. The boundary layer was imaged at seven streamwise positions spaced 4 cm apart. At each position, 400 frames were acquired in four 100-frame bursts at 1000 fps, with bursts spaced one second apart to account for any long time-series fluctuations that may occur in the boundary layer. Measurements were taken at flow speeds of 0.15 m/s (Figure 7) and 0.3 m/s (Figure S2), yielding 11,200 boundary layer profiles in total, which were processed using the digital particle tracking velocimetry (PTV) code described by Anderson et al.[8]

ASSOCIATED CONTENT

Data Availability Statement

All data needed to evaluate the conclusions in the paper are present in the paper. Additional data related to this paper may be requested from the authors.

Supporting Information

The Supporting Information is available free of charge at https://pubs.acs.org/doi/10.1021/acs.chemmater.6c01113.

Experimental setup images and videos; boundary layer shear stress data; rheological fluid shear stress data; lubricant depletion data (PDF)

Static lift and drag testing of a SLIPS-coated aluminum plate across a range of angles of attack, imaged from below the flow tank (Movie S1) (MP4)

List item dynamic (flapping) propulsion testing of aluminum sample plate (Movie S2) (MP4)

AUTHOR INFORMATION

Corresponding Author

Joanna Aizenberg − *Wyss Institute for Biologically Inspired Engineering, Harvard University, Boston, Massachusetts 02115, United States; John A. Paulson School of Engineering and Applied Sciences, Harvard University, Allston, Massachusetts 02134, United States; Department of Chemistry and Chemical Biology, Harvard University, Cambridge, Massachusetts 02138, United States;* orcid.org/0000-0002-2343-8705; Email: jaiz@seas.harvard.edu

Authors

Jack Alvarenga − *Wyss Institute for Biologically Inspired Engineering, Harvard University, Boston, Massachusetts 02115, United States; John A. Paulson School of Engineering and Applied Sciences, Harvard University, Allston, Massachusetts 02134, United States;* orcid.org/0000-0002-7131-5945

Mughees Khan − *Wyss Institute for Biologically Inspired Engineering, Harvard University, Boston, Massachusetts 02115, United States;* Present Address: Center for Nanoscale Systems, Harvard University, Cambridge, MA 02138, USA

Patrick J. M. Thornycroft − *Department of Organismic and Evolutionary Biology, Harvard University, Cambridge, Massachusetts 02138, United States*

Dylan K. Wainwright − *Department of Organismic and Evolutionary Biology, Harvard University, Cambridge,*

https://doi.org/10.1021/acs.chemmater.6c01113
Chem. Mater. XXXX, XXX, XXX−XXX

Massachusetts 02138, United States; Present Address: Department of Biological Sciences, Purdue University, West Lafayette, IN 47907, USA.

Li Wen − *Department of Organismic and Evolutionary Biology, Harvard University, Cambridge, Massachusetts 02138, United States;* Present Address: School of Mechanical Engineering and Automation, Beihang University, Beijing, 100191, China.

Erik J. Anderson − *Department of Mechanical Engineering, Grove City College, Grove City, Pennsylvania 16127, United States*

Philseok Kim − *Wyss Institute for Biologically Inspired Engineering, Harvard University, Boston, Massachusetts 02115, United States;* orcid.org/0000-0001-5814-2675

George V. Lauder − *Department of Organismic and Evolutionary Biology, Harvard University, Cambridge, Massachusetts 02138, United States*

Complete contact information is available at: https://pubs.acs.org/10.1021/acs.chemmater.6c01113

Author Contributions

M.K, J.Ai., L.W., and G.V.L. conceived the paper. M.K., J.Al., and P.K. fabricated the coated aluminum plates. L.W., P.J.M.T., E.J.A., and M.K. conducted the static and dynamic measurements in the flow tank. P.J.M.T., J.Al., and L.W. analyzed the data. J.Al., M.K., and D.K.W. contributed to the viscosity measurements. P.J.M.T., G.V.L., L.W., E.J.A., M.K., J.Al., and J.Ai. interpreted the data and wrote the manuscript. All authors have given approval to the final version of the manuscript.

Notes

The authors declare no competing financial interest.

■ ACKNOWLEDGMENTS

The authors would like to thank Tom Blough for aluminum plate machining and technical support. This work was supported by ONR Award #N00014-25-1-2128 to J. Aizenberg, ONR MURI Grant N00014-14-1-0533 to G.V.L.

■ REFERENCES

(1) Costerton, J. W.; Lewandowski, Z.; Caldwell, D. E.; Korber, D. R.; Lappin-Scott, H. M. Microbial Biofilms. *Annu. Rev. Microbiol.* **1995**, *49* (49), 711−745.
(2) Kaliner, M.; Marom, Z.; Patow, C.; Shelhamer, J. Human Respiratory Mucus. *J. Allergy Clin. Immunol.* **1984**, *73* (3), 318−323.
(3) Bohn, H. F.; Federle, W. Insect aquaplaning: Nepenthes pitcher plants capture prey with the peristome, a fully wettable water-lubricated anisotropic surface. *Proc. Natl Acad. Sci. USA* **2004**, *101*, 14138−14143.
(4) Wainwright, D. K.; Lauder, G. V. Mucus Matters: The Slippery and Complex Surfaces of Fish. In *Functional Surfaces in Biology III*; Biologically-Inspired Systems, Gorb, S.; Gorb, E., Eds.; Springe: Cham, 2017; Vol. *10*, pp. 223−246. DOI: .
(5) Shephard, K. L. Functions for Fish Mucus. *Rev. Fish Biol. Fish.* **1994**, *4* (4), 401−429.
(6) Daniel, T. L. FISH MUCUS: *IN SITU* MEASUREMENTS OF POLYMER DRAG REDUCTION. *Biol. Bull.* **1981**, *160* (3), 376−382.
(7) Denny, M. W. Mechanical Properties of Pedal Mucus and Their Consequences for Gastropod Structure and Performance. *Am. Zool.* **1984**, *24* (1), 23−36.
(8) Anderson, E. J.; Mcgillis, W. R.; Grosenbaugh, M. A. The Boundary Layer of Swimming Fish. *J. Exp. Biol.* **2001**, *204* (1), 81−102.
(9) Xu, Z.; Parra, D.; Gómez, D.; Salinas, I.; Zhang, Y.-A.; Von Gersdorff Jørgensen, L.; Heinecke, R. D.; Buchmann, K.; LaPatra, S.; Sunyer, J. O. Teleost Skin, an Ancient Mucosal Surface That Elicits Gut-like Immune Responses. *Proc. Natl. Acad. Sci. U. S. A.* **2013**, *110* (32), 13097−13102.
(10) Bernadsky, G.; Sar, N.; Rosenberg, E. Drag Reduction of Fish Skin Mucus: Relationship to Mode of Swimming and Size. *J. Fish Biol.* **1993**, *42* (5), 797−800.
(11) Tian, F.-B. Hydrodynamic Effects of Mucus on Swimming Performance of an Undulatory Foil by Using the DSD/SST Method. *Comput. Mech.* **2020**, *65* (3), 751−761.
(12) Zhang, Y.; Feng, X.; Tian, G.; Jia, C. Rheological Properties and Drag Reduction Performance of Puffer Epidermal Mucus. *ACS Biomater. Sci. Eng.* **2022**, *8* (2), 460−469.
(13) Wainwright, D. K.; Lauder, G. V.; Gemmell, B. J. Hydrodynamic Function of the Slimy and Scaly Surfaces of Teleost Fishes. *Integr. Comp. Biol.* **2024**, *64* (2), 480−495.
(14) Chen, L.; Zhang, N.; Cui, F.; Wang, H.; Xu, Y.; Liu, C.; Cui, H.; Wu, L. Numerical Investigation of Coupled Drag Reduction Mechanism of Loach Mucus Trapped by Flexible V-Microgrooves. *Phys. Fluids* **2025**, *37*, 081819.
(15) Lee, S. J.; Kim, H. N.; Choi, W.; Yoon, G. Y.; Seo, E. A Nature-Inspired Lubricant-Infused Surface for Sustainable Drag Reduction. *Soft Matter* **2019**, *15* (42), 8459−8467.
(16) Zhao, P.; Li, X.; Luo, Z.; Zhai, Q.; Tian, Y.; Zhang, K.; Guo, H. A Bio-Inspired Drag Reduction Method of Bionic Fish Skin Mucus Structure. *Micromachines* **2024**, *15* (3), 364.
(17) Luo, Z.; Jia, X.; Zhu, S.; Zhao, P.; Zhang, K.; Guo, H. A Bio-Inspired Two-Stage Bionic Drag Reduction Method. *Rev. Sci. Instrum.* **2024**, *95* (3), 035118.
(18) Wainwright, D. K.; Lauder, G. V. Three-Dimensional Analysis of Scale Morphology in Bluegill Sunfish, Lepomis Macrochirus. *Zoology* **2016**, *119* (3), 182−195.
(19) Wainwright, D. K.; Lauder, G. V.; Weaver, J. C. Imaging Biological Surface Topography *in Situ* and *in Vivo*. *Methods Ecol. Evol.* **2017**, *8* (11), 1626−1638.
(20) Fischer, M. J.; Lauder, G. V.; Wainwright, D. K. Slippery and Smooth Shark Skin: How Mucus Transforms Surface Texture. *J. Morphol.* **2025**, *286* (4), No. e70046.
(21) Yan, M.; Gu, Y.; Ma, L.; Tang, J.; He, C.; Zhang, J.; Mou, J. Slime-Groove Drag Reduction Characteristics and Mechanism of Marine Biomimetic Surface. *Appl. Bionics Biomech.* **2022**, *2022*, 1−19.
(22) Wang, S.; Ryu, J.; He, G.-Q.; Qin, F.; Sung, H. J. A Self-Propelled Flexible Plate with a Navier Slip Surface. *Phys. Fluids* **2020**, *32* (2), 021906.
(23) Lauder, G. V.; Tytell, E. D. Hydrodynamics of Undulatory Propulsion. *Fish Physiol.* **2005**, *23*, 425−468.
(24) Di Santo, V.; Goerig, E.; Wainwright, D. K.; Akanyeti, O.; Liao, J. C.; Castro-Santos, T.; Lauder, G. V. Convergence of Undulatory Swimming Kinematics across a Diversity of Fishes. *Proc. Natl. Acad. Sci. U. S. A.* **2021**, *118* (49), No. e2113206118.
(25) Lauder, G. V.; Wainwright, D. K.; Domel, A. G.; Weaver, J. C.; Wen, L.; Bertoldi, K. Structure, Biomimetics, and Fluid Dynamics of Fish Skin Surfaces. *Phys. Rev. Fluids* **2016**, *1* (6), 060502.
(26) Wong, T.-S.; Kang, S. H.; Tang, S. K. Y.; Smythe, E. J.; Hatton, B. D.; Grinthal, A.; Aizenberg, J. Bioinspired Self-Repairing Slippery Surfaces with Pressure-Stable Omniphobicity. *Nature* **2011**, *477* (7365), 443−447.
(27) Wong, T.-S. Engineering Slippery Surfaces. *Annu. Rev. Mater. Res.* **2026**, *56* (1), 207−233.
(28) Kim, P.; Wong, T.-S.; Alvarenga, J.; Kreder, M. J.; Adorno-Martinez, W. E.; Aizenberg, J. Liquid-Infused Nanostructured Surfaces with Extreme Anti-Ice and Anti-Frost Performance. *ACS Nano* **2012**, *6* (8), 6569−6577.
(29) Kreder, M. J.; Alvarenga, J.; Kim, P.; Aizenberg, J. Design of Anti-Icing Surfaces: Smooth, Textured or Slippery? *Nat. Rev. Mater.* **2016**, *1* (1), 15003.
(30) Leslie, D. C.; Waterhouse, A.; Berthet, J. B.; Valentin, T. M.; Watters, A. L.; Jain, A.; Kim, P.; Hatton, B. D.; Nedder, A.; Donovan, K.; Super, E. H.; Howell, C.; Johnson, C. P.; Vu, T. L.; Bolgen, D. E.; Rifai, S.; Hansen, A. R.; Aizenberg, M.; Super, M.; Aizenberg, J.; Ingber, D. E. A Bioinspired Omniphobic Surface Coating on Medical Devices

Prevents Thrombosis and Biofouling. *Nat. Biotechnol.* **2014**, *32* (11), 1134−1140.
(31) Amini, S.; Kolle, S.; Petrone, L.; Ahanotu, O.; Sunny, S.; Sutanto, C. N.; Hoon, S.; Cohen, L.; Weaver, J. C.; Aizenberg, J.; Vogel, N.; Miserez, A. Preventing Mussel Adhesion Using Lubricant-Infused Materials. *Science* **2017**, *357* (6352), 668−673.
(32) Kolle, S.; Ahanotu, O.; Meeks, A.; Stafslien, S.; Kreder, M.; Vanderwal, L.; Cohen, L.; Waltz, G.; Lim, C. S.; Slocum, D.; Greene, E. M.; Hunsucker, K.; Swain, G.; Wendt, D.; Teo, S. L.-M.; Aizenberg, J. On the Mechanism of Marine Fouling-Prevention Performance of Oil-Containing Silicone Elastomers. *Sci. Rep.* **2022**, *12* (1), 11799.
(33) Epstein, A. K.; Wong, T.-S.; Belisle, R. A.; Boggs, E. M.; Aizenberg, J. Liquid-Infused Structured Surfaces with Exceptional Anti-Biofouling Performance. *Proc. Natl. Acad. Sci. U. S. A.* **2012**, *109* (33), 13182−13187.
(34) Lee, J.; Shin, S.; Jiang, Y.; Jeong, C.; Stone, H. A.; Choi, C. Oil-Impregnated Nanoporous Oxide Layer for Corrosion Protection with Self-Healing. *Adv. Funct. Mater.* **2017**, *27* (15), 1606040.
(35) Pakzad, H.; Nouri-Borujerdi, A.; Moosavi, A. Studying Liquid-Infused Surfaces with Affordable Surface Features Infiltrated with Various Lubricants from Corrosion, Biofouling, and Fluid Drag Viewpoints. *Langmuir* **2023**, *39* (31), 10978−10992.
(36) Solomon, B. R.; Khalil, K. S.; Varanasi, K. K. Drag Reduction Using Lubricant-Impregnated Surfaces in Viscous Laminar Flow. *Langmuir* **2014**, *30* (36), 10970−10976.
(37) Rosenberg, B. J.; Van Buren, T.; Fu, M. K.; Smits, A. J. Turbulent Drag Reduction over Air- and Liquid- Impregnated Surfaces. *Phys. Fluids* **2016**, *28* (1), 015103.
(38) Van Buren, T.; Smits, A. J. Substantial Drag Reduction in Turbulent Flow Using Liquid-Infused Surfaces. *J. Fluid Mech.* **2017**, *827*, 448−456.
(39) Kim, S. J.; Kim, N. K.; Lee, S. J.; Sung, H. J. A Lubricant-Infused Slip Surface for Drag Reduction. *Phys. Fluids* **2020**, *32*, 091900.
(40) Kim, P.; Kreder, M. J.; Alvarenga, J.; Aizenberg, J. Hierarchical or Not? Effect of the Length Scale and Hierarchy of the Surface Roughness on Omniphobicity of Lubricant-Infused Substrates. *Nano Lett.* **2013**, *13* (4), 1793−1799.
(41) Mazare, A.; Ulubas, M. H.; Kim, H.; Fomicheva, I.; Sarau, G.; Christiansen, S. H.; Goldmann, W. H.; Tesler, A. B. Binding Kinetics of Self-Assembled Monolayers of Fluorinated Phosphate Ester on Metal Oxides for Underwater Aerophilicity. *Langmuir* **2025**, *41* (3), 1868−1875.
(42) Woodward, J. T.; Ulman, A.; Schwartz, D. K. Self-Assembled Monolayer Growth of Octadecylphosphonic Acid on Mica. *Langmuir* **1996**, *12* (15), 3626−3629.
(43) Thissen, P.; Valtiner, M.; Grundmeier, G. Stability of Phosphonic Acid Self-Assembled Monolayers on Amorphous and Single-Crystalline Aluminum Oxide Surfaces in Aqueous Solution. *Langmuir* **2010**, *26* (1), 156−164.
(44) Spori, D. M.; Venkataraman, N. V.; Tosatti, S. G. P.; Durmaz, F.; Spencer, N. D.; Zürcher, S. Influence of Alkyl Chain Length on Phosphate Self-Assembled Monolayers. *Langmuir* **2007**, *23* (15), 8053−8060.
(45) Wan, X.; Lieberman, I.; Asyuda, A.; Resch, S.; Seim, H.; Kirsch, P.; Zharnikov, M. Thermal Stability of Phosphonic Acid Self-Assembled Monolayers on Alumina Substrates. *J. Phys. Chem. C* **2020**, *124* (4), 2531−2542.
(46) Hoque, E.; DeRose, J. A.; Hoffmann, P.; Mathieu, H. J.; Bhushan, B.; Cichomski, M. Phosphonate Self-Assembled Monolayers on Aluminum Surfaces. *J. Chem. Phys.* **2006**, *124* (17), 174710.
(47) Li, L.; Lin, Y.; Rabbi, K. F.; Ma, J.; Chen, Z.; Patel, A.; Su, W.; Ma, X.; Boyina, K.; Sett, S.; Mondal, D.; Tomohiro, N.; Hirokazu, F.; Miljkovic, N. Fabrication Optimization of Ultra-Scalable Nanostructured Aluminum-Alloy Surfaces. *ACS Appl. Mater. Interfaces* **2021**, *13* (36), 43489−43504.
(48) Van Den Brand, J.; Snijders, P. C.; Sloof, W. G.; Terryn, H.; De Wit, J. H. W. Acid−Base Characterization of Aluminum Oxide Surfaces with XPS. *J. Phys. Chem. B* **2004**, *108* (19), 6017−6024.
(49) Kummert, R.; Stumm, W. The Surface Complexation of Organic Acids on Hydrous Y-AI203. *J. Colloid Interface Sci.* **1980**, *75* (2), 373−385.
(50) Liascukiene, I.; Aissaoui, N.; Asadauskas, S. J.; Landoulsi, J.; Lambert, J.-F. Ordered Nanostructures on a Hydroxylated Aluminum Surface through the Self-Assembly of Fatty Acids. *Langmuir* **2012**, *28* (11), 5116−5124.
(51) López, C.; Galmés, B.; Soberats, B.; Frontera, A.; Rotger, C.; Costa, A. Surface Modification of Pseudoboehmite-Coated Aluminum Plates with Squaramic Acid Amphiphiles. *ACS Omega* **2019**, *4* (12), 14868−14874.
(52) Hoshino, M.; Kimachi, Y.; Terada, A. Thermogravimetric Behavior of Perfluoropolyether. *J. Appl. Polym. Sci.* **1996**, *62* (1), 207−215.
(53) Kvíčala, J. Chemistry and Applications of Perfluoro- and Polyfluoroethers. In *The Curious World of Fluorinated Molecules*; Elsevier, 2021; pp. 319−342. .
(54) Triantafyllou, G. S.; Triantafyllou, M. S.; Grosenbaugh, M. A. Optimal Thrust Development in Oscillating Foils with Application to Fish Propulsion. *J. Fluids Struct.* **1993**, *7* (2), 205−224.
(55) Read, D. A.; Hover, F. S.; Triantafyllou, M. S. Forces on Oscillating Foils for Propulsion and Maneuvering. *J. Fluids Struct.* **2003**, *17* (1), 163−183.
(56) Lauder, G. V.; Madden, P. G. A. Fish Locomotion: Kinematics and Hydrodynamics of Flexible Foil-like Fins. *Exp. Fluids* **2007**, *43* (5), 641−653.
(57) Lauder, G. V.; Tangorra, J. L. Fish Locomotion: Biology and Robotics of Body and Fin-Based Movements. In *Robot Fish − Bio-inspired Fishlike Underwater Robots*; Springer: Berlin, 2015; pp. 25−49. DOI: .
(58) Lauder, G. V.; Lim, J.; Shelton, R.; Witt, C.; Anderson, E.; Tangorra, J. L. Robotic Models for Studying Undulatory Locomotion in Fishes. *Mar. Technol. Soc. J.* **2011**, *45* (4), 41−55.
(59) Shelton, R. M.; Thornycroft, P. J. M.; Lauder, G. V. Undulatory Locomotion of Flexible Foils as Biomimetic Models for Understanding Fish Propulsion. *J. Exp. Biol.* **2014**, *217*, 2110−2120.
(60) Yanase, K.; Saarenrinne, P. Unsteady Turbulent Boundary Layers in Swimming Rainbow Trout. *J. Exp. Biol.* **2015**, *218*, 1373−1385.
(61) Xu, M.; Grabowski, A.; Yu, N.; Kerezyte, G.; Lee, J.-W.; Pfeifer, B. R.; Kim, C.-J. "Cj." Superhydrophobic Drag Reduction for Turbulent Flows in Open Water. *Phys. Rev. Appl.* **2020**, *13* (3), 034056.
(62) Lee, C.; Choi, C.-H.; Kim, C.-J. Superhydrophobic Drag Reduction in Laminar Flows: A Critical Review. *Exp. Fluids* **2016**, *57* (12), 176.
(63) Xu, M.; Sun, G.; Kim, C.-J. Infinite Lifetime of Underwater Superhydrophobic States. *Phys. Rev. Lett.* **2014**, *113* (13), 136103.
(64) Bartolo, D.; Bouamrirene, F.; Verneuil, E.; Buguin, A.; Silberzan, P.; Moulinet, S. Bouncing or Sticky Droplets: Impalement Transitions on Superhydrophobic Micropatterned Surfaces. *Europhys. Lett.* **2006**, *74* (2), 299−305.
(65) Kim, H. N.; Kim, S. J.; Choi, W.; Sung, H. J.; Lee, S. J. Depletion of Lubricant Impregnated in a Cavity of Lubricant-Infused Surface. *Phys. Fluids* **2021**, *33* (2), 022005.
(66) Alinovi, E.; Bottaro, A. Apparent Slip and Drag Reduction for the Flow over Superhydrophobic and Lubricant-Impregnated Surfaces. *Phys. Rev. Fluids* **2018**, *3* (12), 124002.
(67) Zhang, K.; Zhang, C.; Jiang, W.; Zhang, J. Stability and Drag Reduction Mechanism of Mucus-Water Interface on Underwater Vehicle Surface. *Phys. Fluids* **2025**, *37* (2), 022150.
(68) Vega-Sánchez, C.; Peppou-Chapman, S.; Zhu, L.; Neto, C. Nanobubbles Explain the Large Slip Observed on Lubricant-Infused Surfaces. *Nat. Commun.* **2022**, *13* (1), 351.
(69) Peppou-Chapman, S.; Vega-Sánchez, C.; Neto, C. Detection of Nanobubbles on Lubricant-Infused Surfaces Using AFM Meniscus Force Measurements. *Langmuir* **2022**, *38* (33), 10234−10243.
(70) Vega-Sánchez, C.; Neto, C. Fluid Slip and Drag Reduction on Liquid-Infused Surfaces under High Static Pressure. *Langmuir* **2024**, *40* (8), 4460−4467.

https://doi.org/10.1021/acs.chemmater.6c01113
Chem. Mater. XXXX, XXX, XXX−XXX

(71) James, L.; Gresham, I. J.; Schnell, G.; Seitz, H.; Neto, C. Effect of Surface-Lubricant Compatibility on Bubble Formation in Lubricant-Infused Surfaces. *Adv. Mater. Interfaces* **2026**, *13* (8), No. e70446.
(72) Yang, H.; Zeng, B.; Zhang, X.; Xing, Y.; Gui, X.; Cao, Y. Control of Boundary Slip by Interfacial Nanobubbles: A Perspective from Molecular Dynamics Simulations. *Phys. Fluids* **2023**, *35* (3), 032108.
(73) Park, G. D.; Lee, S. J. Exploiting High Gas Content in Lubricants to Enhance Drag Reduction on Lubricant-Infused Surfaces. *Phys. Fluids* **2025**, *37* (6), 062116.
(74) Hawkes, J. W. The Structure of Fish Skin: I. General Organization. *Cell Tissue Res.* **1974**, *149* (2), 147−158.
(75) Parrish, J. K.; Kroen, W. K. Sloughed Mucus and Drag-Reduction in a School of Atlantic Silversides, Menidia Menidia. *Mar. Biol.* **1988**, *97* (2), 165−169.
(76) Nair, R. A.; Chandran, N. K.; Ranjith, S. K. Hydrodynamic Drag Reduction in Ribbed Microchannel with Infused Non-Newtonian Lubricants. *Phys. Fluids* **2024**, *36* (1), 012022.
(77) Oeffner, J.; Lauder, G. V. The Hydrodynamic Function of Shark Skin and Two Biomimetic Applications. *J. Exp. Biol.* **2012**, *215* (5), 785−795.
(78) Bixler, G. D.; Bhushan, B. Bioinspired Micro/Nanostructured Surfaces for Oil Drag Reduction in Closed Channel Flow. *Soft Matter* **2013**, *9* (5), 1620−1635.
(79) Neto, C.; Evans, D. R.; Bonaccurso, E.; Butt, H.-J.; Craig, V. S. J. Boundary Slip in Newtonian Liquids: A Review of Experimental Studies. *Rep. Prog. Phys.* **2005**, *68* (12), 2859−2897.
(80) Blevins, E.; Lauder, G. V. Swimming near the Substrate: A Simple Robotic Model of Stingray Locomotion. *Bioinspir. Biomim.* **2013**, *8* (1), 016005.
(81) Tytell, E. D.; Lauder, G. V. The Hydrodynamics of Eel Swimming. *J. Exp. Biol.* **2004**, *207* (11), 1825−1841.
(82) Drucker, E. G.; Lauder, G. V. Locomotor Function of the Dorsal Fin in Rainbow Trout: Kinematic Patterns and Hydrodynamic Forces. *J. Exp. Biol.* **2005**, *208* (23), 4479−4494.
(83) Lucas, K. N.; Thornycroft, P. J. M.; Gemmell, B. J.; Colin, S. P.; Costello, J. H.; Lauder, G. V. Effects of Non-Uniform Stiffness on the Swimming Performance of a Passively-Flexing, Fish-like Foil Model. *Bioinspir. Biomim.* **2015**, *10* (5), 056019.
(84) Feilich, K. L.; Lauder, G. V. Passive Mechanical Models of Fish Caudal Fins: Effects of Shape and Stiffness on Self-Propulsion. *Bioinspir. Biomim.* **2015**, *10* (3), 036002.

https://doi.org/10.1021/acs.chemmater.6c01113
Chem. Mater. XXXX, XXX, XXX−XXX